Fibers and Polymers 2022, Vol.23, No.3, 711-719
DOI 10.1007/s12221-022-3218-0

ISSN 1229-9197 (print version)
ISSN 1875-0052 (electronic version)

Aramid Nanofibers Reinforced Polyacrylonitrile Nanocomposite Films with High Transparency and High Mechanical Properties

Xue Bai[1], Yinghui Zhao[1], Zhenhu Song[2], Hui Chen[1], Sihang Zhang[1], Yonghui Luo[1], Yingchun Gu[1], Shijian Tu[2], Guo Yao[1]*, and Sheng Chen[1]*

[1]*College of Biomass Science and Engineering, National Engineering Laboratory for Clean Technology of Leather Manufacture, Sichuan University, Chengdu 610065, China*
[2]*Zhonghao Chenguang Research Institute of Chemistry Industry, Fushun 643201, China*
(Received March 2, 2021; Revised May 11, 2021; Accepted June 16, 2021)

Abstract: The preparation of polymer nanocomposites combined with high strength, toughness, and high transparency remains a challenge. Aramid fibers are often used as fiber-reinforced materials for their superior mechanical and thermal properties, but the weak interfacial force between aramid fibers and matrix polymer limits the application in composite materials. In this work, aramid nanofibers were prepared by a two-step process, which included deprotonation and acid hydrothermal treatment to obtain better dispersions in general solvents. The hydrothermal aramid nanofibers (HANFs) were used as reinforcing materials and blended with polyacrylonitrile (PAN) to prepare polyacrylonitrile/aramid nanofibers (PAN/HANFs) composite films with different mass fractions of HANFs. The morphologies of HANFs and the thermal, optical, and mechanical properties of composite films were investigated. Interestingly, when the mass fraction of aramid nanofibers was less than 1.0 %, the composite films were synchronously strengthened and toughened. When the mass fraction of HANFs was 0.5 %, the tensile strength and toughness of the PAN/HANFs composite film reached 62.04 MPa and 22.56 MJ/m^3, which were 74.23 % and 162.31 % higher than the pure PAN film, respectively. Besides, its average transmittance in the visible light region remained 76.34 %. This work may offer a novel and facile strategy for high transparent reinforced polymer composites, which have potential applications in high strength fiber or optical film.

Keywords: Aramid nanofibers, Polyacrylonitrile, Fiber reinforced polymer composites, Polymer films, Mechanical properties

Introduction

For the development of new materials, much effort has been committed to develop novel light-weight materials with ultrahigh mechanical properties [1-3]. Fiber-reinforced (such as carbon fiber, glass fiber, high strength organic fiber, and so on) composites have the characteristics of high specific strength, large specific modulus, light weight, and anisotropy, which are the research hotspots in the field of composite materials at present [4-6]. Especially, poly(paraphenylene terephthalamide), a kind of aramid fiber, commonly known by its trade-name Kevlar, is one kind of high-performance fiber with outstanding mechanical properties and excellent thermal properties [7,8], which has been widely used in shipbuilding, aircraft, automotive, aerospace, sports, fire prevention applications, and so on [9-11]. Kevlar has been regarded as the most important organic reinforcing fiber for advanced composite materials via its high strength, high modulus, and low density. However, due to the weak interfacial force between Kevlar and matrix polymer, the mechanical properties of the composites prepared by direct blending are limited [12,13].

Nanofibers have a small size effect because of their ultra-high specific surface area, which are expected to bring distinctive properties different from bulk materials, such as extremely excellent mechanical properties [14,15], unique optical properties [16], extra energy harvesting [17] and strong interaction [18]. As reinforcing materials, nanofibers can significantly increase the contact area between the fillers and the polymer matrix to enhance the interfacial force for the components of composite materials [19,20]. Jiang *et al*. [21] used nylon-6 nanofibers to reinforce the melamine-formaldehyde (MF)/nylon-6 composite materials by electrostatic spinning, and the interfacial forces between MF and nylon-6 enhanced the mechanical properties of composites. In addition, nanofibers can also be used to obtain transparent composites. Devarayan *et al*. [22] prepared a nylon nanofiber-reinforced cellulose acetate film for flexible electrodes, which showed transparency from 39 % to 82 %. Based on the superior mechanical properties and thermal stability of aramid nanofibers, using aramid nanofibers as reinforcing materials is expected to improve the mechanical or thermal properties of composites. Kotov's team at the University of Michigan developed a facile preparation method of aramid nanofibers (ANFs) first. They used ANFs as a "building block" and obtained several functional composites [23,24]. For instance, gold nanoparticles (Au NPs) were incorporated into a porous aramid nanofibers matrix, which reduced the charge percolation threshold and facilitated charge transport, to achieve materials with high electrical conductivity [25].

Polyacrylonitrile (PAN) is a kind of polymer with high activity and easy modification which is widely used in

*Corresponding author: yaoguo@scu.edu.cn
*Corresponding author: chensheng@scu.edu.cn

textile, filtration, adsorption, catalysis, and other fields [26-28]. However, PAN materials have low strength, poor fatigue resistance, and high brittleness, which limit their application. Beril Melbiah *et al*. [29] prepared a flat sheet PAN-based plate ultrafiltration membrane that mixed amphiphilic copolymer Pluronic F127 with inorganic calcium carbonate nanoparticles by non-solvent induced phase transformation. However, the PAN-based ultrafiltration membrane had a very low tensile strength (less than 3.1 MPa). Therefore, developing the PAN materials with higher strength and toughness can further expand their application. For all we know, there is no report on using aramid nanofibers as additives to reinforce PAN films at present. In this paper, Kevlar fibers were used as raw materials to prepare hydrothermal aramid nanofibers (HANFs) with good dispersion by deprotonation and acid hydrothermal methods. As the reinforcing materials, HANFs were blended with PAN in DMF solution to prepare polyacrylonitrile/aramid nanofibers (PAN/HANFs) composite films with low contents of HNAFs ranged from 0.1 % to 1.0 %. The morphologies of aramid nanofibers and the optical, thermal, and mechanical properties of PAN/HANFs composite films were characterized by transmission electron microscopy (TEM), Fourier transformed infrared spectrum (FTIR), ultraviolet-visible spectrum, thermogravimetry (TG), differential scanning calorimetry (DSC), and strength tester. The results showed that PAN/HANFs composite films not only maintained the original transparency but also simultaneously improved the strength and toughness, which were 74.23 % and 162.31 % higher than those of the pure PAN film, respectively.

Experimental

Materials

Kevlar 49 was provided by Dupont, USA. Dimethyl sulfoxide (DMSO) was provided by Tianjin Fuyu fine chemical Company Limited, China. Polyacrylonitrile (PAN) with a molecular weight of 85000 was provided by Shaoxing Jema Composite Materials Company Limited, China. N,N-dimethyl Formamide (DMF), Potassium hydroxide (KOH), Sulfuric acid (H_2SO_4), and Nitric acid (HNO_3) were all provided by Kelong Chemical Company Limited, Chengdu, China. During the process of experiment, deionized water was employed.

Preparation of Hydrothermal Aramid Nanofiber (HANFs) Dispersion

Firstly, 100 mg of Kevlar 49 fibers and 150 mg potassium hydroxide (KOH) were added into 50 m*l* dimethyl sulfoxide (DMSO) and stirred magnetically at room temperature (25 °C) for one week to obtain a dark red ANFs/DMSO dispersion. Then, the obtained ANFs/DMSO dispersion was dispersed into deionized water, followed by filtrating and washing repeatedly. Next, the solid was hydrothermally treated with mixed aqueous solution of sulfuric acid and nitric acid (the concentrations of H_2SO_4 and HNO_3 were 37.5 wt% and 8.75 wt%, respectively) in a Teflon-lined autoclave at 120 °C for 2 h. After cooling down, the product was filtrated and washed with deionized water to pH=7.0. Then the above solid was freeze-dried to obtain hydrothermal aramid nanofibers (HANFs). Finally, the HANFs were ultrasonicated 30 min in the organic solvent N,N-dimethylformamide (DMF) for use.

Preparation of PAN/HANFs Composites Film

As shown in Figure 1, a simple blending casting method was used to prepare PAN/HANFs nanocomposite films. Firstly, 250 mg of PAN power was dissolved in 50 m*l* of DMF solution, under the same total mass, PAN/DMF and HANFs/DMF were mixed and stirred at different mass ratios for 2 h. The obtained dispersion was treated with ultrasound

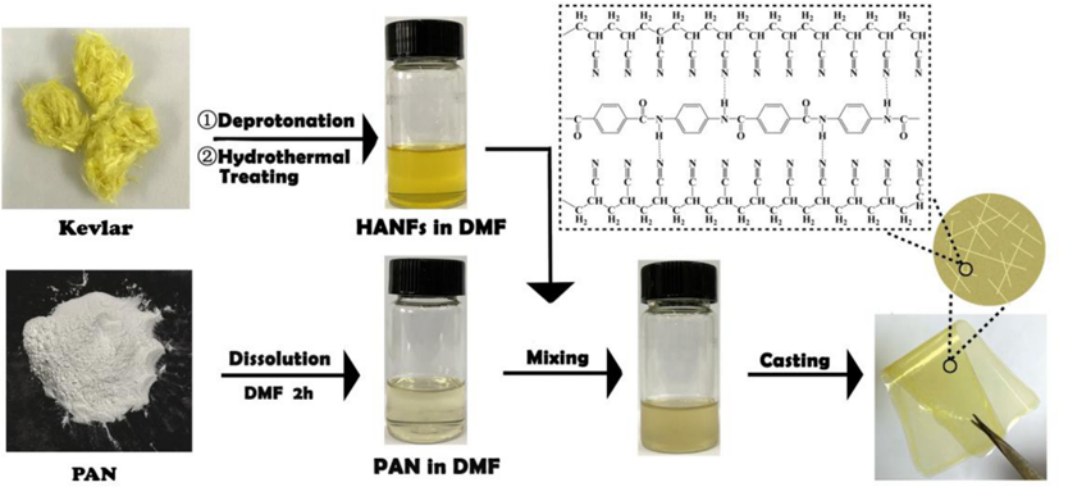

Figure 1. Fabrication process of PAN/HANFs composite films.

for 30 minutes and rested for 2 h to degas. The mixtures were poured into a glass mold to form films, after natural air drying, the films were dried in a vacuum environment of 60 °C for 24 hours to obtain the final composite films. The mass fractions of HANFs in the composite films were 0.0 %, 0.1 %, 0.2 %, 0.5 %, 0.8 % and 1.0 %, respectively.

Characterization

The morphologies of ANFs and HANFs were observed by Tecnai G2 F20 S-TWIN transmission electron microscopy (FEI, USA), and the average diameters of nanofibers were calculated by Nano Measurer. And the cross-section morphologies of pure PAN film and 0.5 % PAN/HANFs film were observed by JSM-5900LV scanning electron microscopy (JEOL, Japan). The optical transmittances of the nanocomposite films were measured by UV-1800 (Beijing Purkinje General Instrument Company Limited). The Fourier transformed infrared spectra of the composite films were tested by Tracer100 infrared spectrometer (Shimadzu Corporation, Japan). The thermal gravimetric analysis of PAN, HANFs, and PAN/HANFs composite films were carried out at 30-600 °C under nitrogen at a heating rate of 20 °C/min by DTA-60 thermogravimeter (Shimadzu, Japan). The differential scanning calorimetry (DSC) of PAN, HANFs, and PAN/HANFs composite films were analyzed at 30-400 °C with a heating rate of 20 °C/min under nitrogen by DSC 214Polyma differential scanning calorimeter (Netzsch, Germany). For the mechanical property tests, the composite films with different aramid nanofibers mass fractions were cut into test samples of 3 cm in length and 1 mm in width. The thicknesses were measured by thickness gauge, and the tensile test was carried out by strength meter (ly-06b, Laizhou electronic instrument Company Limited). The average values of the strength were obtained from 5 tests for each sample. The toughnesses (K) were determined from the stress (σ)-strain (ε) curves. According to the method reported in the literature [30], toughnesses were calculated using the equation (1),

$$K = \sum_{i=0}^{n} \sigma \varepsilon_i \quad (1)$$

where σ and ε respectively referred to the tensile stress and strain at failure. The Young's modulus was calculated by the formula (2),

$$E = \frac{F \cdot L}{A \cdot \Delta L} = \sigma / \varepsilon \quad (2)$$

where F/A (σ) and $\Delta L/L$ (ε) respectively referred to the force per unit area and relative deformation under external forces.

Results and Discussion

Morphology

To obtain a high-performance composite, fillers with good dispersibility, high strength, and high specific surface areas are intensively required, which are well satisfied by nanofibers of high strength polymers. In this work, hydrothermal aramid nanofibers were prepared by a two-step process (Figure 2), which included deprotonation and hydrothermal acid hydrolysis. Figure 3(a) and (b) were the TEM image and diameter statistical distribution diagram of the aramid nanofibers (ANFs) prepared by the deprotonation method. It showed that the ANFs had a one-dimensional fibrous structure, and the average diameter of the fibers was

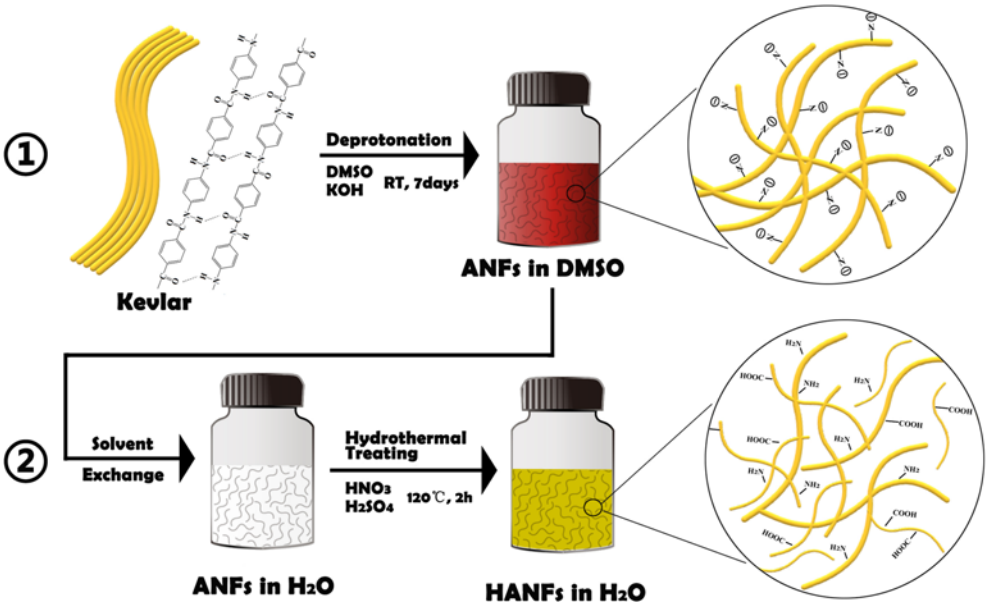

Figure 2. Schematic illustration of the preparation of HANFS nanofibers by a two-step process.

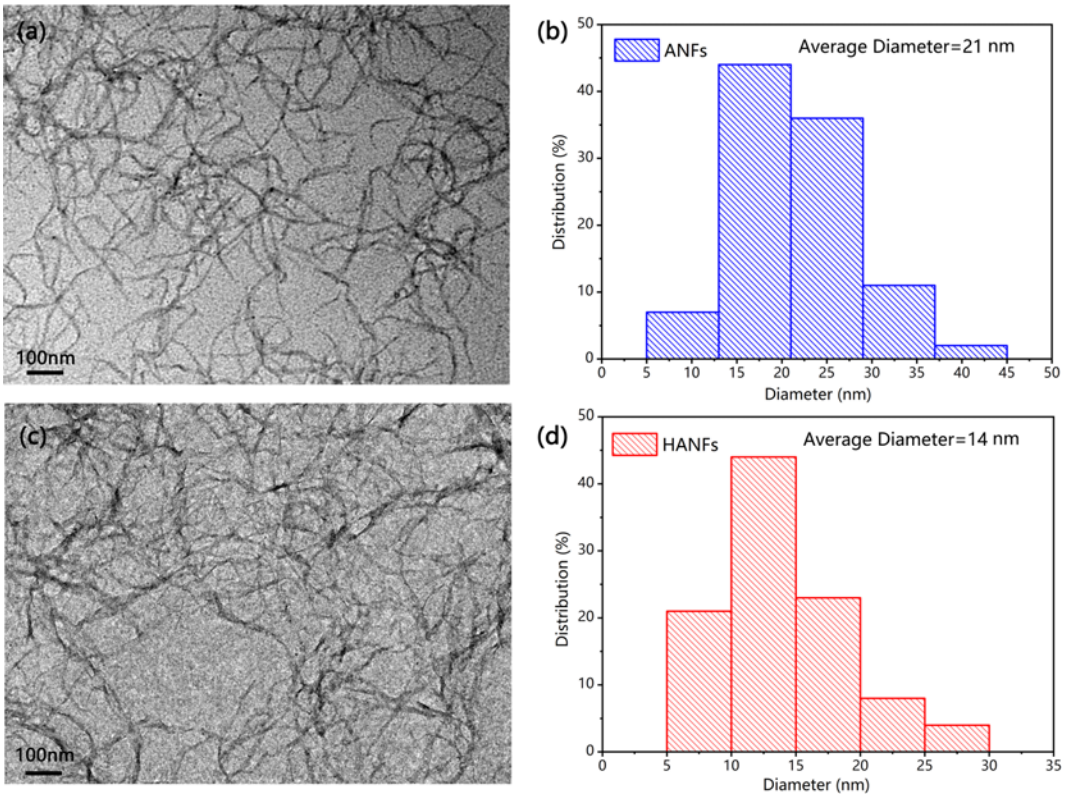

Figure 3. (a) TEM image of ANFs, (b) average diameter of ANFs, (c) TEM image of HANFs, and (d) average diameter of HANFs.

about 22 nm, indicating that aramid nanofibers can be successfully prepared through the deprotonation process. In the deprotonation process, partial hydrogen atoms on the aromatic polyamide bonds were captured under the action of KOH, so the -NH- group was deprotonated and became negatively charged. However, in the DMSO/KOH system, DMSO was an aprotic solvent and cannot provide protons. Therefore, aramid fibers were split into a nano-meter level and formed stable homogeneous dispersion by electrostatic repulsion between the polyamide molecular chains [31]. However, the nanofibers prepared by the first-step could not be well dispersed into other solvent systems except DMSO. So, the hydrothermal acid hydrolysis treatment was adopted for further modification. Figure 3(c) and (d) showed the TEM image and diameter statistical distribution diagram of HANFs, which were obtained after hydrothermal acid hydrolysis treatment and could disperse well in common polar solvents. The HANFs still maintained the nanofibrous structure like ANFs, but the average diameter of HANF was about 14 nm, which was obviously lower than that of the ANFs. The possible reason should be that the ANFs were hydrolyzed and oxidized slightly by the hydrothermal treatment and more polar groups exposed on the surface of the nanofibers, which greatly improved the dispersion of aramid nanofibers in other solvents (Figure 1).

FTIR Study of Composites Films

In order to confirm the structural changes of ANFs caused by hydrothermal treatment, Fourier transform infrared spectra of ANFs before and after hydrothermal treatment were tested. As shown in Figure 4, the peaks at 1018 and 820 cm^{-1} corresponded to the in-plane and out-of-plane C-H vibration of the benzene ring, respectively [32,33]. The absorption intensity of these two peaks did not change significantly after the hydrothermal treatment. However, the absorption intensities of peaks at 1542, 1516, and 1320 cm^{-1} increased obviously. The first two peaks were attributed to the vibration absorption of N-H [34]. The last peak was induced by the Ph-N vibration. In addition, the absorption intensity of stretching vibration of C=O at 1658 cm^{-1} also increased. Furthermore, two new weak peaks appeared at the wavenumbers of 1154 and 1452 cm^{-1} of the FTIR curve of HANFs, which were attributed to the absorption bands of carboxylic acids and hydroxyl groups. The above results indicated that after hydrothermal treatment, the polymers on the surface of the ANFs were degraded in a certain degree. So more polar groups were produced and exposed on the surface of the nanofibers.

The spectrum of pure PAN film showed typical absorbance bands at 2241 cm^{-1}, which was the stretching vibration of C≡N, and the absorption peak at 1730 cm^{-1} was

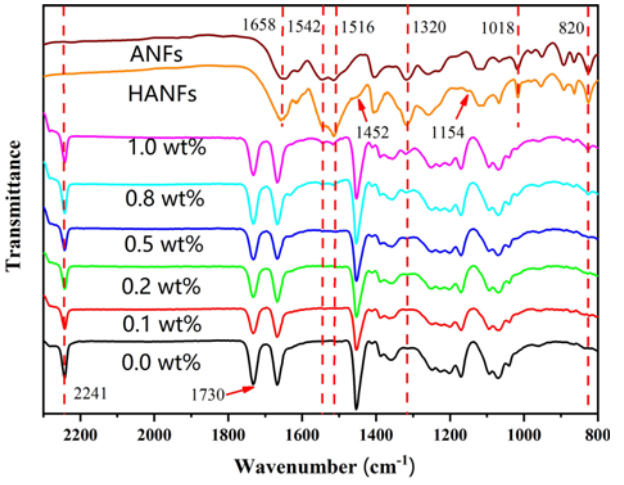

Figure 4. FTIR spectra of ANFs, HANFs, PAN film, and PAN/HANFs composite films with different amounts of HANFs content.

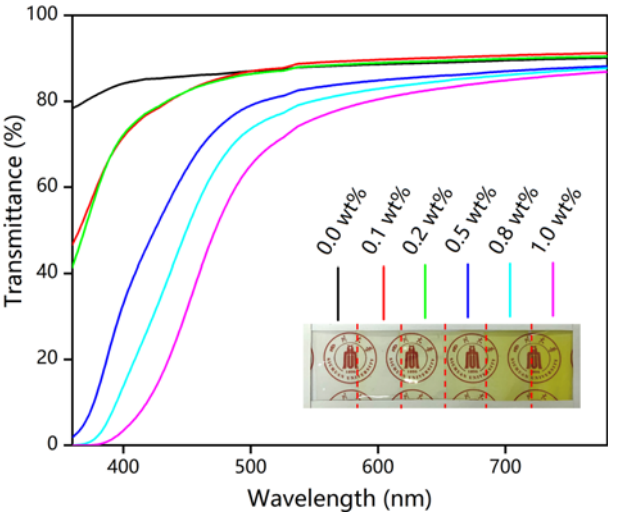

Figure 5. Transmittance curves of pure PAN film and PAN/HANFs composite films with different amounts of HANFs contents, and the inset shows the photographs of all films.

the stretching vibration of C=O bond [35]. In the FTIR of the composite films, characteristic absorption peaks of PAN could be seen obviously. With the increase of HANFs contents, the characteristic absorption peaks of HANFs at 1542, 1516, 1320, 1018, and 820 cm^{-1} could be observed in the FTIR curves of PAN/HANFs composite films, indicating that HANFs had been successfully incorporated with PAN matrix.

Optical Transmittance Analysis

Polymer films with good transparency have many potential applications in food packaging, flexible display, screen film, biomedical and so on [36]. But most fiber-reinforced composites are opaque or translucent because of their bi-phase structure, which limits their application. Through reducing the size of the dispersed particles and making them smaller than the wavelength of visible light, the nanoscale fillers can keep the transparency of the polymer matrix. Here, the composite films with good transparency were obtained by mixing well dispersed HANFs with PAN. Figure 5 showed the ultraviolet-visible spectra and photographs of the pure PAN film and PAN/HANFs composite films with different mass fractions. As shown in the inset, the color of the composite films deepened with the increase of the mass fraction of aramid nanofibers, and the background pattern could be seen clearly through the films. This indicated that HANFs could be well dispersed in the films without obvious agglomeration phenomenon, leading to the formation of uniform and homogeneous composite.

In the visible wavelength range (380-780 nm), the transmittance of composite films decreased with the increase of the mass fraction of aramid nanofibers. To characterize the optical transmittance of composite films, a performance index called average transmittance (T_{ave}) was introduced here. T_{ave} was defined as the average visible light transmittance of 380 to 780 nm, which provided a method for understanding the optical properties of materials. According to the reported method [37], the calculation formula was expressed by equation (3),

$$T_{ave} = \Sigma_{\lambda=380}^{780} T_{\lambda}/(780-380) \quad (3)$$

where λ was the measured wavelength. The calculation results were shown in Table 1. With the addition of HANFs, the average transmittance of composite films decreased, but all of them were above 64 %. When the contents of nanofibers were less than 0.5 %, the T_{ave} values higher than 76 %, and the transmittances between 500 nm and 780 nm were about 80 %. Above results indicated that the PAN/HANFs nanocomposite films demonstrate an excellent optical transparency.

Table 1. Average transmittance of pure PAN film and PAN/HANFs composite films with different amounts of HANFs content

Films	PAN	0.1 wt%	0.2 wt%	0.5 wt%	0.8 wt%	1.0 wt%
T_{ave} (%)	88.03	86.78	86.25	76.34	70.86	64.98

Thermal Stabilities

The thermal stability of aramid fibers is better than most of the organic fibers, which make it be an ideal reinforcing material for heat-resistant composite materials. To study the effect of HANFs on the thermal performance of PAN/HANFs composite films, thermogravimetric analysis was conducted on the pure PAN, HANFs, and PAN/HANFs

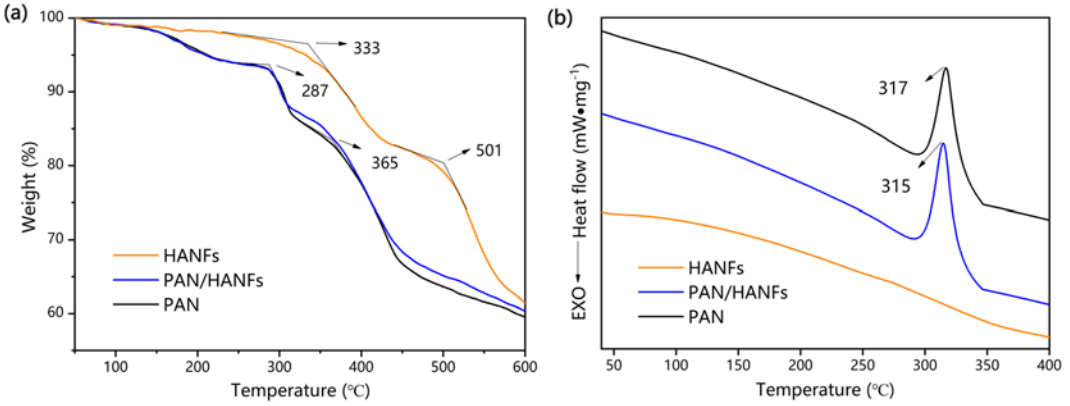

Figure 6. (a) TGA and (b) DSC curves of HANFs, PAN and 0.5 wt% PAN/HANFs film.

composite films under nitrogen atmosphere. As shown in the weight loss curve of HANFs (Figure 6a), there was a small mass loss before 100 °C, which was caused by the evaporation of a small amount of water in the nanofibers. There were two major zones of weight loss between 300-600 °C. The first weight loss below 450 °C should be the release of oligomers formed during the hydrothermal process. The second weight loss was observed in the temperature range from 500 to 600 °C, which was estimated by the degradation of poly(paraphenylene terephthalamide) main chains of HANFs [33]. The residual char content of HANFs at 600 °C was nearly 60.79 %, which was consistent with Kevlar fibers [38]. It indicated that HANFs could maintain good thermal stability of their raw materials after the hydrothermal treatment. The thermogravimetric curves of pure PAN film and PAN/HANFs composite film were similar and showed weight loss in three stages. The first, slow weight loss from 150 up to 200 °C should be attributed to the dehydration and desorption of a small amount of water and residual DMF solvent molecules [39]. The second stage started at 287 °C and ended at 320 °C, which was associated with the cyclization of nitrile groups in the PAN polymer chain [40, 41]. In the third stage, from about 365 to 450 °C, the decomposition of the PAN main chain was presented. When further heating to 600 °C, the char yield was about 58.94 %. For the PAN/HANFs composite film of containing 0.5 %, the final residual char yield was a little higher than the pure PAN film.

The thermal properties of composite films also were evaluated by differential scanning calorimetry in a nitrogen atmosphere (Figure 6b). As shown in the figure, the DSC curve of HANFs did not show any endothermic or exothermic peaks, indicating its thermal stability in the testing temperature range. The DSC curve of pure PAN film showed a wide exothermic peak in the range of 291 to 347 °C, which was attributed to the reactions of PAN-cyclization of nitrile groups and dehydrogenation [42]. The peak temperature was at 317 °C, which represented the maximum exothermic temperature of pure PAN. The temperature range of aforementioned exothermic peak was consistent with the TG cure of pure PAN film (Figure 6a). For the 0.5 % PAN/HANFs composite film, the initial exothermic temperature and maximum exothermic temperature were 287 °C and 315 °C, respectively. Both of them were a little lower than the pure PAN film, which should be attributed to the conformational disorder with the addition of nanofillers [43].

Mechanical Properties

As an organic reinforcement, aramid fibers have excellent mechanical properties, which are widely used in many applications in which high strength and modulus, and high impact resistance are required. More importantly, the high specific surface area of HANFs prepared in this work could increase the contact interfacial area between the reinforced material and the matrix, leading to the increase of its interface force, which would greatly improve the mechanical properties of PAN/HANFs composite films. The typical stress-strain curves, Young's modulus, tensile strength, toughness, and elongation at break of PAN film and PAN/HANFs nanocomposite films were illustrated in Figure 7. Interestingly, the addition of HANFs had simultaneously increased the strength and modulus of PAN films. Figure 7(b) showed the tensile strength of 35.61 MPa and Young's modulus of 0.56 GPa for the pure PAN film. The PAN/HANFs composite film with a mass fraction of 0.5 % showed the best mechanical properties with the tensile strength of 62.04 MPa and Young's modulus of 0.80 GPa, which were about 74.23 % and 43.14 % higher than the pure PAN film, respectively. The results showed that HANFs were very effective as the nano reinforcing fillers. On the one hand, HANFs possessed large surface areas and good dispersity, which could significantly increase the contact areas between HANFs and PAN matrix. When the external force was transferred to the interior through the interface, the reinforcing nanofibers could distribute the tensile stress

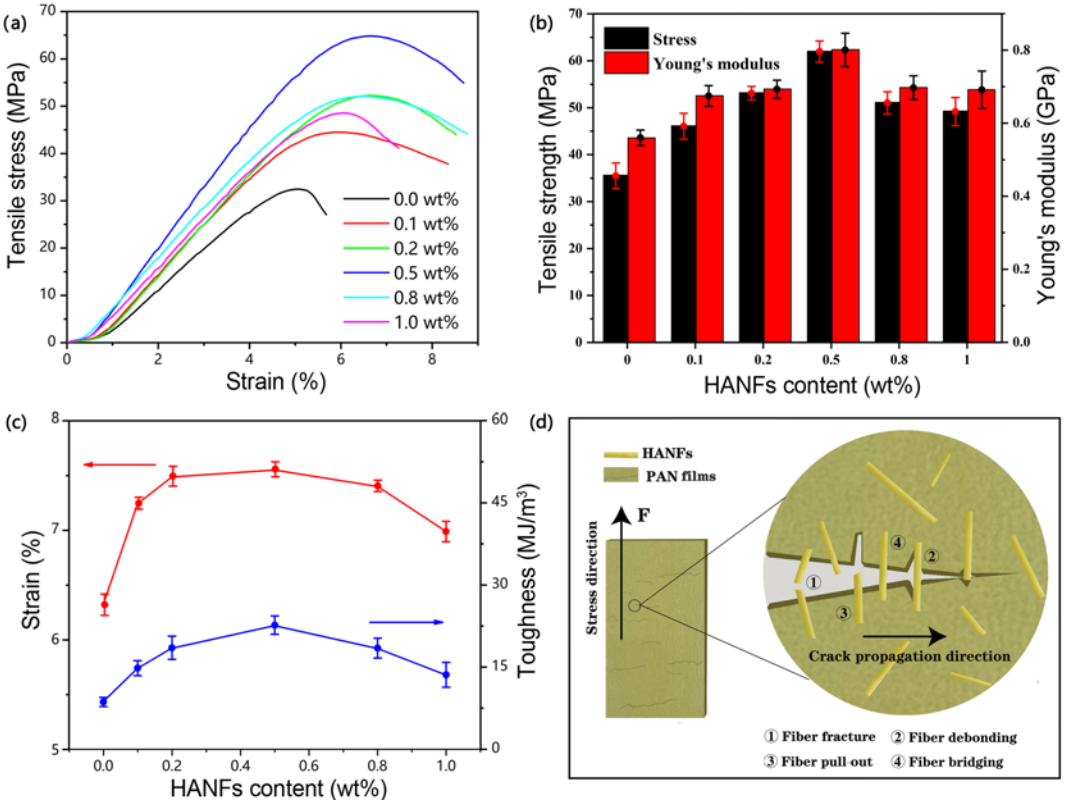

Figure 7. (a) Typical stress-strain curves, (b) tensile strength values and Young's modulus, (c) elongation at break and toughness values, and (d) four kinds of fiber toughening mechanisms.

more even and avoid the concentration of stresses. On the other hand, hydrogen bond interaction between HANFs and PAN would also enhance the resistance of fracture.

It is well known that the strength and toughness are generally mutually exclusive for most materials [44]. However, there is a strong demand for obtaining the materials with both high strength and high toughness [45]. Encouragingly, these two properties of PAN/HANFs composite films were both improved in this work. As shown in Figure 7(c), when the mass fraction of HANFs was 0.5 %, the elongation at break of the PAN/HANFs composite film reached 7.55 %, which was 19.37 % larger than that of the pure PAN film. More importantly, the toughness of the composite film reached 22.56 MJ/m^3, while that of the pure PAN film was 8.60 MJ/m^3, yielding a 162.31 % increase. The possible mechanism of interaction between PAN and HANFs was shown in Figure 7(d). Generally, the energy consumed of the material fracture must be increased as much as possible to improve the toughness of composite materials. As a reinforcement, HANFs had characteristics of high strength and high modulus, which were dispersed in the PAN matrix to bear part of the stress and provided part of energy consumption for the fracture [46]. This phenomenon of energy release was related to the ability of HANFs to alter the microstructure and mechanical behaviors of the composites [47]. In addition, there were four mechanisms could explain the toughening effects: fiber fracture, fiber debonding, fiber pull-out, and fiber bridging [48,49]. Under the action of external force, the matrix of PAN/HANFs composite film cracked or even tore along the direction of tension. Part of HANFs broke in this process, which could consume some energy. Moreover, part of HANFs closed to the front of the crack may be debonding with the PAN matrix before fracture and a new surface generated, which also consumed some energy. The other HANFs closed to the crack tip slid out along the interface of the PAN matrix under the action of external stress, which relaxed the stress at the crack tip and the crack propagation was slowed down. Fiber pull-out required an external force to do work, which also played a role in toughening. Along the direction of crack diffusion, some HANFs closed to the crack tip possibly were not broken, and the fiber bridges were built at both ends of the film crack. These bridges would generate compressive stress on the crack surfaces to counteract the effect of external tensile stress. The fiber bridges could delay the failure of composite films and effectively prevent the crack growth during the tensile process. In addition, more functional groups were exposed on the surface of the hydrothermal aramid nanofibers, resulting in stronger and more stable interfacial interaction between PAN and

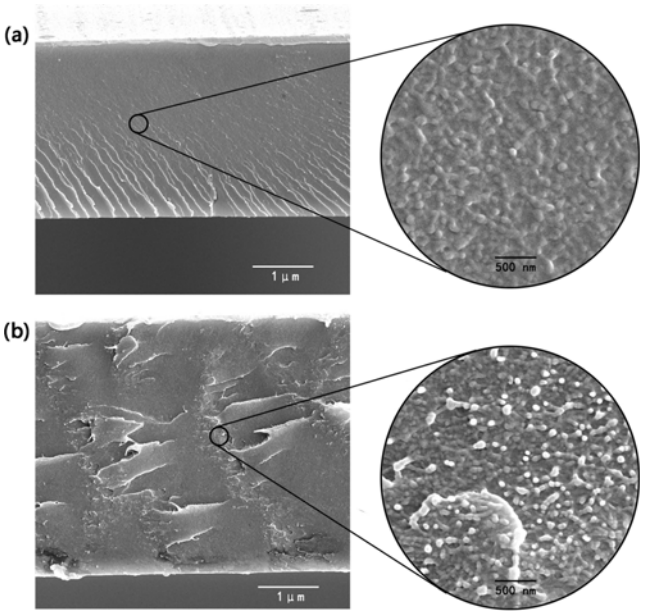

Figure 8. (a) Cross-section morphology of pure PAN film and (b) and 0.5 wt% PAN/ HANFS film.

HANFs, which required more energy to fracture under external forces. It also had a toughening effect.

The above mechanisms could be further confirmed by SEM images of the cross section of the films. The Figure 8(a) and (b) showed the cross-section morphology of pure PAN film and 0.5 % PAN/ HANFS film after direct tensile fracture, respectively. The fracture surface of pure PAN film was smooth and flat, and the roughness of the whole fracture surface increased after the addition of HANFs. Moreover, it could be seen distinctly that the PAN matrix was obviously pulled out with HANFs fibers, and the SEM image shows uniform white spots, indicating that HANFs were evenly distributed in the matrix and had a strong binding force with the PAN matrix.

The HANFs with good dispersity and ultra-high specific surface area, accompanied with above toughening effects and possible hydrogen bonds, can effectively enhance the mechanical properties of PAN films with a small addition amount. However, when the content of HANFs was higher than 0.8 %, the mechanical properties of the composite films decreased instead. It may be due to the self-agglomeration of nanofillers, which resulted in stress concentration and phase separation [50,51]. This is a kind of typical phenomenon for the polymer composites reinforced with nanoscale fillers [52].

Conclusion

In summary, hydrothermal aramid nanofibers with an average diameter of about 14 nm were successfully prepared by two steps method of deprotonation and hydrothermal treatment. When HANFs were used as nano reinforcement of PAN, the transparent PAN/HANFs composite films with both excellent strength and toughness were fabricated by a simple solution casting approach. More importantly, very small amount of HANFs could significantly improve the mechanical properties of the composite films. The optimal tensile strength and toughness were obtained after addition of only 0.5 % HANFs, which were 74.23 % and 162.31 % higher than that of the pure PAN film, respectively. Moreover, its average transmittance value was above 75 % over the entire visible light range. This report provided a novel and facile strategy to achieve high transparent reinforced polymer composites and open a new way for the application of aramid nanofibers.

Acknowledgement

This work was supported by the Science and Technology Cooperation Project of Sichuan University and Zigong City (2019CDZG-3), the Science and Technology Foundation of Sichuan province (2020YFG0094 and 2020YFG0104), and Miaozi Project in Science and Technology Innovation Program of Sichuan Province (No.20-YCG045). We would like to thank the Analytical & Testing Center of Sichuan University for structured illumination microscopy work, and we are grateful to Shanlin Wang for her help with TEM images. We thank Erhui Ren for the experimental assistance.

References

1. X. F. Zhang, Q. W. Li, T. G. Holesinger, P. N. Arendt, J. Y. Huang, P. D. Kirven, T. G. Clapp, R. F. DePaula, X. Z. Liao, Y. H. Zhao, L. X. Zheng, D. E. Peterson, and Y. T. Zhu, *Adv. Mater.,* **19**, 4198 (2007).
2. N. Behabtu, C. C. Young, D. E. Tsentalovich, O. Kleinerman, X. Wang, A. W. K. Ma, E. A. Bengio, R. F. ter Waarbeek, J. J. de Jong, R. E. Hoogerwerf, S. B. Fairchild, J. B. Ferguson, B. Maruyama, J. Kono, Y. Talmon, Y. Cohen, M. J. Otto, and M. Pasquali, *Science*, **339**, 182 (2013).
3. M. Khalifa, S. Janakiraman, S. Ghosh, A. Venimadhav, and S. Anandhan, *Polym. Compos.,* **40**, 2320 (2019).
4. S. Eksi and K. Genel, *Acta Phys. Pol. A*, **132**, 879 (2017).
5. R. Sen, B. Zhao, D. Perea, M. E. Itkis, H. Hu, J. Love, E. Bekyarova, and R. C. Haddon, *Nano Lett*., **4**, 459 (2004).
6. Z. H. Wang, Y. Si, C. Y. Zhao, D. Yu, W. Wang, and G. Sun, *ACS Appl. Mater. Interfaces*, **11**, 27200 (2019).
7. S. Ifuku, H. Maeta, H. Izawa, M. Morimoto, and H. Saimoto, *RSC Adv.,* **4**, 40377 (2014).
8. M. Mortier, P. Moldenaers, and J. Mewis, *Rheol. Acta*, **35**, 57 (1996).
9. J. C. Fan, Z. X. Shi, L. Zhang, J. L. Wang, and J. Yin, *Nanoscale*, **4**, 7046 (2012).
10. J. M. Zhang, Z. Mousavi, N. Soykeabkaew, P. Smith, T. Nishino, and T. Peijs, *ACS Appl. Mater. Interfaces*, **2**, 919

(2010).
11. I. O'Connor, H. Hayden, J. N. Coleman, and Y. K. Gun'ko, *Small*, **5**, 466 (2009).
12. J. J. Lin, S. H. Bang, M. H. Malakooti, and H. A. Sodano, *ACS Appl. Mater. Interfaces*, **9**, 11167 (2017).
13. W. Chen, X. M. Qian, X. Q. He, Z. Y. Liu, and J. P. Liu, *J. Appl. Polym. Sci.,* **123**, 1983 (2012).
14. S. Zhou, G. Zhou, S. Jiang, P. Fan, and H. Hou, *Mater. Lett.,* **200**, 97 (2017).
15. C. B. Huang, S. L. Chen, D. H. Reneker, C. L. Lai, and H. Q. Hou, *Adv. Mater.,* **18**, 668 (2006).
16. Z. J. Ma, Z. L. Hu, H. Zhang, M. Y. Peng, X. He, Y. Li, Z. M. Yang, and J. R. Qiu, *J. Mater. Chem. C*, **4**, 1029 (2016).
17. B. Zaarour, L. Zhu, C. Huang, X.Y. Jin, H. Alghafari, J. Fang, and T. Lin, *J. Ind. Text*., doi.org/10.1177/1528083719870197 (2019).
18. Z. M. Huang, Y. Z. Zhang, M. Kotaki, and S. Ramakrishna, *Compos. Sci. Technol.,* **63**, 2223 (2003).
19. B. M. Wang and C. C. Fan, *J. Nanosci. Nanotechnol.*, **20**, 113 (2020).
20. M. A. Abdelwahab, M. Misra, and A. K. Mohanty, *Ind. Crops Prod.*, **132**, 497 (2019).
21. S. H. Jiang, H. Q. Hou, A. Greiner, and S. Agarwal, *ACS Appl. Mater. Interfaces*, **4**, 2597 (2012).
22. K. Devarayan, D. Y. Lei, H. Y. Kim, and B. S. Kim, *Chem. Eng. J.*, **273**, 603 (2015).
23. M. Yang, K. Q. Cao, L. Sui, Y. Qi, J. Zhu, A. Waas, E. M. Arruda, J. Kieffer, M. D. Thouless, and N. A. Kotov, *ACS Nano*, **5**, 6945 (2011).
24. K. Q. Cao, C. P. Siepermann, M. Yang, A. M. Waas, N. A. Kotov, M. D. Thouless, and E. M. Arruda, *Adv. Funct. Mater.*, **23**, 2072 (2013).
25. J. Lyu, X. Z. Wang, L. H. Liu, Y. Kim, E. K. Tanyi, H. Chi, W. C. Feng, L. Z. Xu, T. H. Li, M. A. Noginov, C. Uher, M. D. Hammig, and N. A. Kotov, *Adv. Funct. Mater.*, **26**, 8435 (2016).
26. J. W. Guo, C. F. Wang, S. H. Chen, J. Y. Lai, C. H. Lu, and J. K. Chen, *Sep. Purif. Technol.,* **234**, 116106 (2020).
27. H. S. Chen, M. H. Huang, Y. B. Liu, L. J. Meng, and M. D. Ma, *Sci Total Environ.*, **739**, 139944 (2020).
28. X. Li, C. Li, G. Y. Gao, B. S. Lv, L. S. Xu, Y. Lu, and G. L. Zhang, *Sci. Total Environ.*, doi.org/10.1016/j.scitotenv.2019.134910 (2020).
29. J. S. B. Melbiah, D. Nithya, and D. Mohan, *Colloids Surf., A*, **516**, 147 (2017).
30. S. Morimune, M. Kotera, T. Nishino, K. Goto, and K. Hata, *Macromolecules*, **44**, 4415 (2011).
31. L. L. Lv, X. S. Han, L. Zong, M. J. Li, J. You, X. C. Wu, and C. X. Li, *ACS Nano*, **11**, 8178 (2017).
32. Y. H. Zhao, S. H. Zhang, F. Hu, J. J. Li, H. Chen, J. Y. Lin, B. Yan, Y. C. Gu, and S. Chen*, J. Mater. Sci.: Mater. Electron*., **30**, 12718 (2019).
33. F. Wang, Y. D. Wu, Y. D. Huang, and L. Liu, *Compos. Sci. Technol.*, **156**, 269 (2018).
34. J. J. Luo, M. Y. Zhang, B. Yang, G. D. Liu, and S. X. Song, *Appl. Nanosci.*, **9**, 631 (2019).
35. J. D. Liu, C. X. Jin, and C. Wang, *J. Colloid Interface Sci.*, **561**, 449 (2020).
36. S. S. Zhang, J. J. Li, Z. P. Yin, X. F. Zhang, S. C. Kundu, and S. Z. Lu, *J. Appl. Polym. Sci.*, **132**, 42407 (2015).
37. C. W. Hu, T. Kawamoto, H. Tanaka, A. Takahashi, K. M. Lee, S. Y. Kao, Y. C. Liao, and K. C. Ho, *J. Mater. Chem. C*, **4**, 10293 (2016).
38. G. M. Cai and W. D. Yu, *J. Therm. Anal. Calorim.*, **104**, 757 (2011).
39. Y. Janowska, T. Mikolajczyk, and M. Bogun, *J. Therm. Anal. Calorim.,* **89**, 613 (2007).
40. H. P. Karki, L. Kafle, D. P. Ojha, J. H. Song, and H. J. Kim, *Sep. Purif. Technol.,* **210**, 913 (2019).
41. Y. Xue, J. Liu, and J. Y. Liang, *Polym. Degrad. Stabil.,* **98**, 219 (2013).
42. Y. Furushima, M. Nakada, H. Takahashi, and K. Ishikiriyama, *Polymer*, **55**, 3075 (2014).
43. A. Kausar and J. Plast, *Film Sheeting*, **35**, 295 (2019).
44. R. O. Ritchie, *Nat. Mater.,* **10**, 817 (2011).
45. Y. Hou, G. L. Zhang, X. P. Tang, Y. Si, X. M. Song, F. X. Liang, and Z. Z. Yang, *Macromolecules*, **52**, 3863 (2019).
46. B. W. Yu, C. Z. Geng, M. Zhou, H. W. Bai, Q. Fu, and B. B. He, *Composites, Part B*, **92**, 413 (2016).
47. A. Jamil, Z. W. Guan, W. J. Cantwell, X. F. Zhang, G. S. Langdon, and Q. Y. Wang, *Int. J. Impact Eng.,* **127**, 31 (2019).
48. Y. T. Zhu, J. A. Valdez, I. J. Beyerlein, S. J. Zhou, C. Liu, M. G. Stout, D. P. Butt, and T. C. Lowe, *Acta Mater.*, **47**, 1767 (1999).
49. D. A. Norman and R. E. Robertson, *J. Appl. Polym. Sci.,* **90**, 2740 (2003).
50. J. W. Shin, J. P. Jeun, and P. H. Kang, *J. Ind. Eng. Chem.*, **15**, 555 (2009).
51. R. Gupta, K. Pancholi, R. De Sa, D. Murray, D. H. Huo, G. Droubi, M. White, and J. Njuguna, *Jom*, **71**, 3119 (2019).
52. L. He and S. C. Tjong, *RSC Adv.*, **5**, 15070 (2015).